Demonstration of a computed-tomography imaging spectrometer using a computer-generated hologram disperser

Michael R. Descour, Curtis E. Volin, Eustace L. Dereniak, Tim M. Gleeson, Mark F. Hopkins, Daniel W. Wilson, and Paul D. Maker

We have constructed a computed-tomography imaging spectrometer that uses a phase-only computer-generated hologram (CGH) array illuminator as the disperser. This imaging spectrometer collects multiplexed spatial and spectral data simultaneously and can be used for flash spectral imaging. The CGH disperser has been designed to maintain nearly equal spectral diffraction efficiency among a 5×5 array of diffraction orders and to minimize diffraction efficiency into higher orders. Reconstruction of the (x, y, λ) image cube from the raw, two-dimensional data is achieved by computed-tomography techniques. The reconstructed image and spectral-signature data compare favorably with measurements by other spectrometric methods. © 1997 Optical Society of America

Key words: Computed-tomography imaging spectrometry, computer-generated holography, disperser design.

1. Introduction

Imaging spectrometry has been demonstrated to be a powerful tool in remote sensing applications since the mid-1980's.[1] Traditional dispersive imaging spectrometers collect (x, y, λ) image-cube data by employing some form of scanning, such as pushbroom scanning (for example, the Hyperspectral Digital Imagery Collection Experiment) or whiskbroom scanning (for example, the Airborne Visible/Infrared Imaging Spectrometer).[2,3] Alternatively, imaging Fourier-transform spectrometers equipped with a focal-plane array (FPA) at the output require scanning of the optical path difference between the two arms of a Michelson interferometer before the image cube can be retrieved from the raw data. Although these methods of data collection are acceptable for stationary or nearly stationary scenes, scanned imaging of dynamic scenes results in artifacts. In the cases of pushbroom or whiskbroom scanning imaging spectrometers, scene motion causes spatial artifacts. In the case of spectrally multiplexing spectrometers, scene motion results in spectral-signature artifacts. The application of computed tomography (CT) in imaging spectrometry is an effective scheme for overcoming these difficulties and for accomplishing instantaneous or flash spectral imaging. The objective of flash spectral imaging is the acquisition of spatial and spectral information about a scene within the shortest possible data-collection time. Imaging applications that call for this form of data acquisition can be found in astronomy, medicine, industrial testing, and defense.

High-signal-to-noise-ratio, high-speed imaging of dynamic events can be accomplished only by a nonscanning imaging spectrometer that maximizes the dwell time at each $(\Delta x, \Delta y, \Delta\lambda)$ image-cube resolution element. A simple concept for such a device is the subject of this paper: A computer-generated two-dimensional (2D) grating disperser is inserted into the collimated beam between lenses that image a system field-stop onto a large-format FPA. The disperser forms a rectangular array of spectrally dispersed images. Each dispersed image can be interpreted as a 2D projection of the three-dimensional (x, y, λ) image cube. Based on such an interpretation, it is possible to reconstruct the (x, y, λ)

M. R. Descour, C. E. Volin, E. L. Dereniak, T. M. Gleeson, and M. F. Hopkins are with the Optical Sciences Center, University of Arizona, Tucson, Arizona 85721. D. W. Wilson and P. D. Maker are with the Center for Space Microelectronics Technology, Jet Propulsion Laboratory, California Institute of Technology, Pasadena, California 91109.

Received 1 August 1996; revised manuscript received 17 December 1996.

0003-6935/97/163694-05$10.00/0

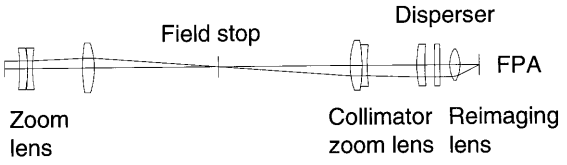

Fig. 1. Instrument layout.

image cube from the array of dispersed images by employing CT algorithms.

The connection between CT and imaging spectrometry was explored in the literature first by Okamoto[4,5] and Bulygin,[6] and later its theoretical and practical limitations were defined by Descour and Dereniak.[7,8] The theoretical limitations may be addressed by a variety of reconstruction constraints, such as positivity or compact support.[9] The practical limitations are related to the radiative throughput of the instrument and, specifically, to the dispersive element. Given a minimum of time for data collection, it is critical that a maximum of the radiation collected by the fore-optics of the imager be detected to maximize signal-to-noise ratio. Loss of light outside the FPA because of high diffraction orders must be minimized. Furthermore, diffraction efficiency that is highly variable among measured diffraction orders can severely reduce the dynamic range of the imaging system. The use of a Dammann grating as a solution to these problems was first suggested by Okamoto.[5] A Dammann grating is a binary-phase diffractive optical element described by transition points between regions of constant phase. In contrast, the computer-generated disperser described in this paper is a pixellated pattern not subject to restrictions on the number of usable phase values at each pixel.

The computed-tomography imaging spectrometer (CTIS) operates over the 450–760-nm spectral range. The spectrometer consists of three optical-element groups: an image-forming optic, a collimator optic, and a reimaging lens. Figure 1 shows two zoom lenses and a short-focal-length lens in each of these roles, respectively. The use of a zoom lens as the collimator allows us to vary the magnification of the field-stop onto the focal plane. Such variation can be used to adjust the effective dispersion within each order.[7,10] The computer-generated hologram (CGH) disperser is located in collimated space between the collimator and the reimaging lens.

A previous version of the CTIS based on crossed thin sinusoidal-phase gratings (XSPGs) as the disperser is described in Refs. 7 and 8. Figures 2(a) and 2(b) show the improved performance of a CGH disperser relative to a XSPG disperser, respectively. The sinusoidal-phase gratings were optimized for maximum diffraction efficiency in the ± 1 orders.[8] In Fig. 2(a), light from a flat-field, broadband source is confined to a 5×5 array of diffraction orders, all of which exhibit a comparable signal level. The same light source was used to generate Fig. 2(b). The central nine diffraction orders are near saturation while the most extreme orders are still only weakly illuminated. The box in Figs. 2(a) and 2(b) indicates the extent of the focal plane (640×640 pixels).

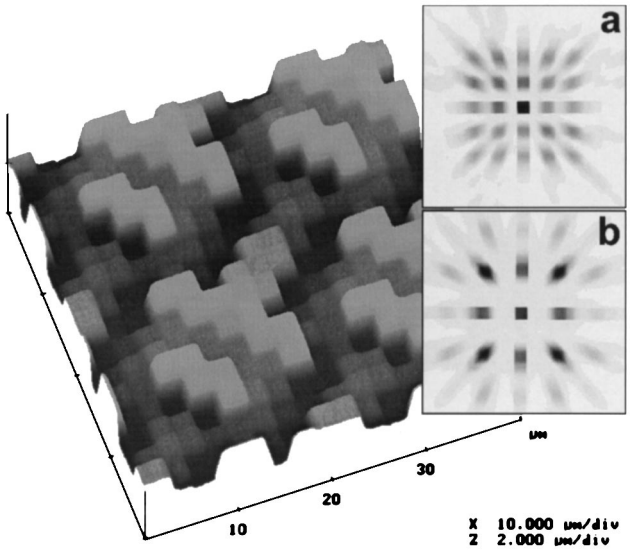

Fig. 2. Atomic force microscope scan of a section of the CGH disperser. a, Measured irradiance distribution on the FPA obtained with the CGH disperser; b, measured irradiance distribution obtained with two crossed sinusoidal-phase gratings as the disperser.

2. Computer-Generated Hologram Disperser Design Algorithm

The 2D grating disperser was designed as an on-axis, phase-only CGH. The design objective was to produce a 5×5 array of equal-irradiance orders with minimal energy diffracted into higher orders. [See Fig. 2(a) for the result of this effort.] The CGH was composed of many replications of an 8×8 array of 2.5×2.5-μm, analog-depth pixels. This resulted in a 20-μm-period 2D grating. The Gerchberg–Saxton algorithm, also known as the Iterative Fourier–Transform algorithm, was used to determine the required pixel depths.[11,12] Because the depths were not constrained to discrete levels, no simulated annealing or random search was required.[12] The design wavelength was chosen to be 585 nm. During the first 50 Gerchberg–Saxton algorithm iterations, orders outside the 5×5 array were constrained to be zero. In subsequent iterations that constraint was removed. This design algorithm produced a disperser with low high-diffraction-order efficiencies as well as a high total diffraction efficiency summed over the desired orders, η_{tot}. The two practical limitations of CT imaging spectrometry mentioned earlier were therefore successfully addressed.

The CGH performance was simulated at wavelengths throughout the CTIS bandwidth. The diffraction efficiencies of the orders did not vary together; i.e., as the wavelength changed, some diffraction orders increased in irradiance while others decreased. Furthermore, this irradiance variation

with wavelength was different for disperser designs developed from different initial random-phase distributions. The initial random-phase distributions are drawn from an infinite design space. Our approach was to search this space by developing many disperser designs and, using a statistical merit function, select the design best suited for the CTIS.

A measure of the uniformity of the irradiance pattern at a particular wavelength λ is the standard deviation of the 25 diffraction efficiencies associated with the 5×5 array of on orders, $\sigma_{on}(\lambda)$. For each disperser design, $\sigma_{on}(\lambda)$ was evaluated at seven wavelengths: $\lambda \in \{450, 501.7, 553.3, 605, 656.7, 708.3, 760\}$. The values of the on orders were scaled so that their mean was unity. The ideal disperser design would result in equal irradiance in each of the 5×5 orders at all tested wavelengths (minimize σ_{on} at each wavelength) and would also exhibit the same value of σ_{on} at all tested wavelengths. We express these preferences through a merit function,

$$f_{merit} = \text{mean}[\sigma_{on}(\lambda_i)] + \text{std}[\sigma_{on}(\lambda_i)] = \frac{1}{N}\sum_{i=1}^{N}\sigma_{on}(\lambda_i) + \left\{\frac{\sum_{i=1}^{N}[\sigma_{on}(\lambda_i) - \langle\sigma_{on}(\lambda_i)\rangle_\lambda]^2}{N-1}\right\}^{1/2}, \quad (1)$$

where the mean and standard deviation (std) are calculated over the seven test wavelengths ($N = 7$). Good disperser designs minimize the value of f_{merit}. The first term in Eq. (1) decreases for disperser designs that maintain the same diffraction efficiency at every one of the 5×5 diffraction orders, and the second term decreases for those disperser designs that maintain consistent performance with varying wavelength.

3. Comparison of Computer-Generated Hologram and Crossed Thin Sinusoidal-Phase Gratings Dispersers

The best CGH disperser design for use in the CTIS was selected from 500 candidate designs and had a calculated merit-function value of 0.335. The worst CGH disperser design had a merit-function value of 0.889. In comparison, the calculated minimum f_{merit} value achievable with a XSPG disperser is 0.958 (zero-to-peak phase delay of 2.25 rad at 632.8 nm). All calculations for thin sinusoidal-phase gratings relied on the analysis in Ref. 13 and were based on the assumption that index of refraction did not vary with wavelength.

Table 1 lists calculated and measured σ_{on} values at three representative wavelengths. These values were obtained for the best CGH disperser and the XSPG disperser described in Ref. 8. In the case of the XSPG disperser, the calculated σ_{on} values were based on a thin sinusoidal-phase grating with a zero-to-peak phase delay of 1.8 rad at 632.8 nm.[8] For derivation of the table's calculated and measured entries, the 25 signal levels in the 5×5 array of diffraction orders [Figs. 2(a) and (b)] were scaled to have unity mean. Given the data in Table 1, the measured CGH disperser σ_{on} values are lower and thus better than the calculated XSPG disperser σ_{on} values by a factor of at least 1.6 and as high as 6.3. The measured CGH disperser σ_{on} values are lower than the corresponding measured XSPG disperser parameters by a factor of at least 1.7 and as high as 6.7. Finally, the calculated minimum σ_{on} for a XSPG disperser is 0.64, corresponding to a zero-to-peak phase delay of 2.8 rad.[13] For the XSPG disperser characterized in Table 1, this minimum occurs at 407 nm, i.e., outside the spectrometer's bandwidth.

Table 1. CGH and XSPG Disperser Measured and Calculated σ_{on} Values[a]

Wavelength (nm)	Best CGH Disperser σ_{on}		XSPG Disperser σ_{on}	
	Calculated	Measured	Calculated	Measured
450	0.45	0.46 ± 0.01	0.76	0.80 ± 0.02
585[b]	1.9×10^{-4}	0.150 ± 0.002	0.95	1.00 ± 0.01
760	0.28	0.47 ± 0.01	0.94	1.11 ± 0.01

[a] σ_{on} dimensionless, unity mean.
[b] CGH design wavelength.

Table 2 compares the calculated and the measured η_{tot} values for the best CGH disperser relative to η_{tot} values calculated for the optimal XSPG disperser ($f_{merit} = 0.958$).

The optimal XSPG offers higher total diffraction efficiency at longer wavelengths compared with the CGH disperser. Total diffraction efficiency must be considered in context of the FPA. If the FPA is a silicon detector array, then higher η_{tot} at shorter wavelengths is more important owing to the low quantum efficiency there. A loss of light, i.e., lower η_{tot}, at the long-wavelength end of the instrument bandwidth can be tolerated because of a much higher quantum efficiency.[14] The CGH disperser therefore offers a more advantageous distribution of η_{tot} with wavelength than does the optimal XSPG disperser, given the data of Table 2. We plan to include η_{tot} into the merit function [Eq. (1)] for future disperser design.

4. Disperser Fabrication

Fabrication of the CTIS disperser was accomplished with Jet Propulsion Laboratory's electron-beam (e-

Table 2. Measured and Calculated η_{tot} values for the CGH Disperser and the Optimal XSPG Disperser

Wavelength (nm)	Calculated Total Diffraction Efficiency η_{tot} (%)		
	Best CGH Disperser Calculated Total	Best CGH Disperser Measured Total	Optimal XSPG Disperser
450	65	65 ± 3	52
585[a]	79	78 ± 5	82
760	72	72 ± 2	95

[a] CGH design wavelength.

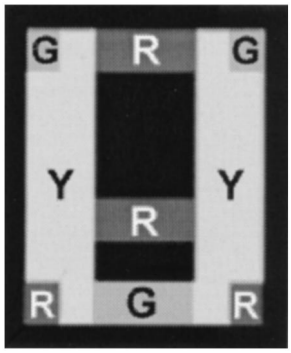

Fig. 3. UA scene used in the spectral-imaging example.

beam) lithography technique for forming analog surface-relief patterns in thin films of poly-(methyl methacrylate) (PMMA).[15,16] Before exposure the depth pattern was converted to e-beam dose, with corrections for the nonlinear dose response of PMMA and the e-beam proximity effect (backscattered dose from the substrate). The pixel pattern was then written in a 2.5-μm-thick layer of PMMA on a quartz substrate with the JEOL JBX-5DII e-beam tool operating at 50 keV. The total hologram was 17 mm in diameter and took 9.6 h to expose at a current of 13.5 nA. Following exposure, the element was developed in pure acetone for approximately 10 s to yield the final surface-relief pattern. An atomic force microscope scan of a section of the surface is shown in Fig. 2.

5. Spectral Imaging Demonstration

Figures 3–5 illustrate an example of spectral imaging with the CGH-based CTIS. The scene consisted of the letters U and A displayed on the green and red phosphors of a color video monitor, respectively.[8] In Fig. 3, different shades of gray denote different colors: Y means yellow, R means red, G means green, and the background appears as black. The CTIS was

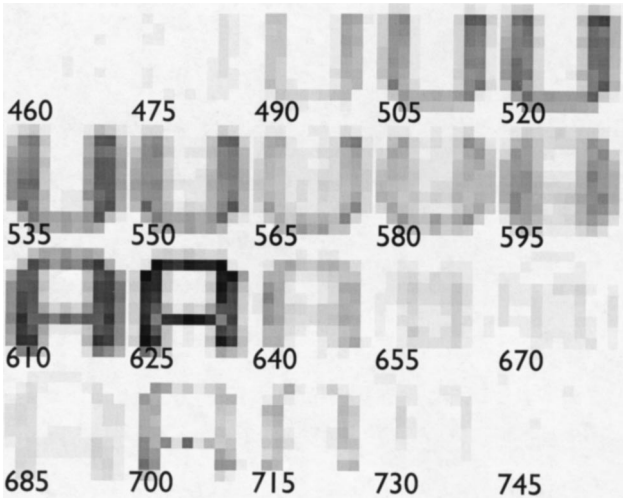

Fig. 4. Spectral slices through the UA image cube reconstructed from the raw data collected by the CGH disperser-based CTIS. Images are shown in negative contrast.

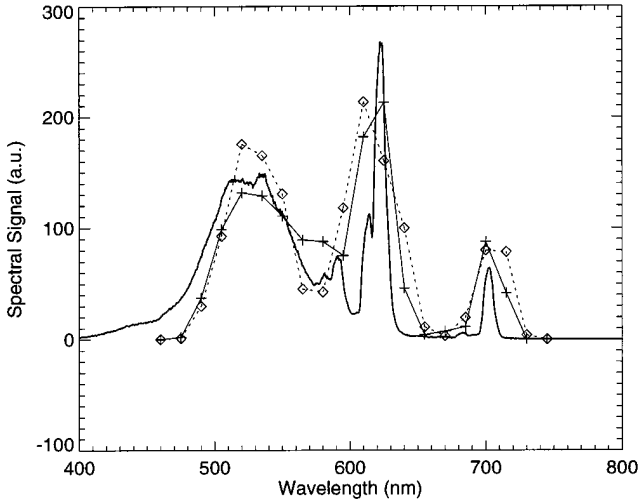

Fig. 5. Comparison of reconstructed and directly measured spectral signatures.

calibrated experimentally, and reconstruction of the (x, y, λ) image cube was accomplished by the expectation–maximization algorithm.[7,8] The numbers in Fig. 4 designate each reconstructed spectral image's center wavelength. The reconstructed spectral images measure 11×11 pixels. Figure 5 compares an example of a reconstructed spectrum to the spectrum measured with a fiber spectrometer (Ocean Optics Model S1000). The measured and reconstructed spectra were taken from a scene region common to both the U and the A (marked Y in Fig. 3). The solid curve traces the fiber-spectrometer-measured spectrum. The + curve indicates the best reconstruction of the target spectrum in the least-squares sense. The ◇ curve represents the worst reconstruction of the target spectrum. For example, note the poorly resolved 700-nm red-phosphor feature. Higher spectral resolution requires that higher diffraction orders be collected on the FPA.[7] Spectral shifts of features and poor fidelity at the short-wavelength end of the instrument bandwidth can be attributed to CTIS calibration errors.[17]

6. Conclusions and Further Work

We have designed and fabricated a multi-phase-level, computer-generated hologram disperser for use in an imaging spectrometer. This disperser offers unprecedented control over spectral diffraction efficiency associated with each diffraction order. In the context of CTIS, this property can be utilized in two ways: (1) the diffraction efficiency can be minimized for diffraction orders beyond a certain order [second order in Fig. 2(a)], and (2) the distribution of spectral irradiance among the collected diffraction orders can be adjusted. The first property means that most of the radiance in the field-stop of the CTIS is actually detected by the FPA, and relatively little of the field-stop spectral exitance propagates at angles that exceed that subtense of the FPA. The second property means that the average irradiance level in each

diffraction order is approximately the same. [As a counter-example, consider Fig. 2(b) and XSPG entries in Table 1.] We have experimentally demonstrated a CTIS using this computer-generated hologram disperser. Higher spectral resolution will require the availability of diffraction orders higher than those contained in the nominal 5×5 array used in the demonstration spectrometer.[7] The design and fabrication of such a disperser is the subject of continuing work.

References

1. A. F. H. Goetz, "Imaging spectrometry for earth remote sensing," Science **228,** 1147–1153 (1985).
2. R. W. Basedow, D. C. Carmer, and M. E. Anderson, "HYDICE system, implementation, and performance," in *Imaging Spectrometry*, M. R. Descour, J. M. Mooney, D. L. Perry, and L. R. B. Illing, eds., Proc. SPIE **2480,** 258–267 (1995).
3. W. M. Porter and H. T. Enmark, "A system overview of the Airborne Visible/Infrared Imaging Spectrometer (A VIRIS)," in *Imaging Spectroscopy II*, G. Vane, ed., Proc. SPIE **834,** 22–31 (1987).
4. T. Okamoto and I. Yamaguchi, "Simultaneous acquisition of spectral image information," Opt. Lett. **16,** 1277–1279 (1991).
5. T. Okamoto, A. Takahashi, and I. Yamaguchi, "Simultaneous acquisition of spectral and spatial intensity distribution," Appl. Spectrosc. **47,** 1198–1202 (1993).
6. F. V. Bulygin, G. N. Vishnyakov, G. G. Levin, and D. V. Karpukhin, "Spectrotomography—a new method of obtaining spectrograms of 2-D objects," Opt. Spectrosc. (USSR) **71,** 561–563 (1991).
7. M. R. Descour, "Non-scanning Imaging Spectrometry," Ph.D. dissertation (University of Arizona, Tucson, Ariz., 1994).
8. M. R. Descour and E. L. Dereniak, "Computed-tomography imaging spectrometer: experimental calibration and reconstruction results," App. Opt. **34,** 4817–4826 (1995).
9. M. I. Sezan and H. Stark, "Applications of convex projection theory to image recovery in tomography and related areas," in *Image Recovery: Theory and Application*, H. Stark, ed. (Academic, San Diego, Calif., 1987), pp. 415–462.
10. P. A. Bernhardt, "Direct reconstruction methods for hyperspectral imaging with rotational spectrotomography," J. Opt. Soc. Am. A **12,** 1884–1901 (1995).
11. R. W. Gerchberg and W. O. Saxton, "A practical algorithm for the determination of phase from image and diffraction plane pictures," Optik **35,** 237–246 (1972).
12. A. F. Gmitro and C. L. Coleman, "Multilevel phase holograms for free-space optical interconnects: design and analysis," in *Optoelectronic Interconnects and Packaging*, R. T. Chen and P. S. Guilfoyle, eds., Proc. SPIE **CR62,** 88–105 (1996).
13. J. W. Goodman, *Introduction to Fourier Optics*, 2nd ed. (McGraw–Hill, New York, 1996), Chap. 4, pp. 81–83.
14. E. L. Dereniak and D. G. Crowe, *Optical Radiation Detectors* (Wiley, New York, 1984), Chap. 9, p. 225.
15. P. D. Maker and R. E. Muller, "Phase holograms in polymethyl methacrylate," J. Vac. Sci. Technol. B **10,** 2516–2519 (1992).
16. P. D. Maker, D. W. Wilson, and R. E. Muller, "Fabrication and performance of optical interconnect analog phase holograms made by electron-beam lithography," in *Optoelectronic Interconnects and Packaging*, R. T. Chen and P. S. Guilfoyle, eds., Proc. SPIE **CR62,** 415–430 (1996).
17. M. R. Descour, R. Schowengerdt, and E. L. Dereniak, "Analysis of the computed-tomography imaging spectrometer by singular value decomposition," in *Algorithms for Multispectral and Hyperspectral Imagery II*, E. Iverson, ed., Proc. SPIE **2758,** 127–133 (1996).